Flat band induced room-temperature ferromagnetism in two-dimensional systems

G. Bouzerar*

Université Grenoble Alpes, CNRS, Institut NEEL, F-38042 Grenoble, France

(Received 26 September 2022; revised 23 May 2023; accepted 24 May 2023; published 30 May 2023)

The remarkable and fascinating properties of two-dimensional (2D) materials have raised them to the rank of most promising candidates for technological applications. In particular, the possibility of long-range ferromagnetic order in 2D materials is generating a growing excitement. Here, we demonstrate that flat bands (FBs) can pave the way for room-temperature ferromagnetism in 2D compounds. Indeed, the magnetic exchanges between localized spins are largely dominated by the FB-FB contribution. This contribution is ferromagnetic and scales linearly with the local coupling, thus leading to crossover temperatures (ferromagnetic phase/paramagnetic phase) higher by an order of magnitude than those currently reported in experiments. High crossover temperatures could be reached in micrometer-sized FB systems.

DOI: 10.1103/PhysRevB.107.184441

Since graphene has been discovered, the interest in two-dimensional material (2DM) has grown tremendously. In the plethora of studies, two areas of research have particularly stood out: flat band (FB) physics, and magnetism in 2DM. In FB systems, the dispersionless bands are at the origin of unforeseen phenomena [1,2] such as fractional quantum Hall states [3,4], unconventional superconductivity [5–7], and magnetism [8–10]. FBs host as well an unusual type of quantum electronic transport as revealed in several studies [11–14]. The interest for ferromagnetism in 2DM such as $Cr_2Ge_2Te_6$, CrI_3 or Fe_3GeTe_2 is experiencing a boost over the past years [15–22]. 2DMs are undoubtedly promising candidates for technological applications, in spintronics, optoelectronics and data storage. Ferromagnetism in 2DMs was long ignored, because of the Mermin-Wagner (MW) theorem [23] that says that in one and two dimensions, continuous symmetries cannot be spontaneously broken at finite temperature in systems with short-range interactions. The MW theorem only excludes long-range magnetic order at finite temperature in the thermodynamic limit, i.e., for infinite systems. However, it does not exclude the possibility of quasi-long-range ordering in finite systems below a crossover temperature T_C^* [24–26]. It implies that below T_C^* the spin-spin correlation length is much larger than the system size. So far, T_C^* reported in micrometer-sized samples has been at most about 40 K which stimulates the search for strategies to gain the missing order of magnitude. Our aim is to discuss the impact of FBs on the magnetic properties of 2D systems. One key question is whether FBs may or may not promote ferromagnetism beyond room temperature. To address this issue, we consider the *s-d* Lieb Model as it is illustrated in Fig. 1. This model describes itinerant carriers locally coupled to localized magnetic spins that are considered classical. We recall that in $Cr_2Ge_2Te_6$ or CrI_3 the spin of Cr^{3+} is $S = 3/2$. The advantages of considering the Lieb lattice (LL) are numerous. First, the LL is a simple square lattice with 3 atoms/unit cell. It possesses a FB at $E = 0$, there is no need to nanostructure or introduce defects or vacancies in the lattice. Finally, it could be designed experimentally in the framework of covalent-organic compounds [27]. The Hamiltonian reads,

$$\widehat{H} = \sum_{\langle ij\rangle,\alpha} (t_{ij} c^{\dagger}_{i\alpha} c_{j\alpha} + \text{H.c.}) + J \sum_{i\in B,C} \widehat{\mathbf{s}}_i \cdot \mathbf{S}_i. \tag{1}$$

$c^{\dagger}_{i\alpha}$ creates an electron with spin $\alpha{=}\uparrow,\downarrow$ at site $\mathbf{R}_i$. In the first term, the sum runs over the lattice sites, $\langle ij\rangle$ are restricted to nearest-neighbor pairs for which the hopping $t_{ij} = -t$. J is the local Kondo coupling between the localized classical spin $\mathbf{S}_i = S.\mathbf{e}_i$ at site $\mathbf{R}_i$ ($\mathbf{e}_i$ being a unit vector) and that of the itinerant carrier $\widehat{\mathbf{s}}_i$. Its components are $\widehat{s}^{\lambda}_i = c^{\dagger}_{i\alpha}[\widehat{\sigma}^{\lambda}]_{\alpha\beta} c_{i\beta}$ where $\lambda = x, y$, and z and $\widehat{\sigma}^{\lambda}$ are the Pauli matrices. In what follows we set $t = 1$ and JS is expressed in units of t. In this study, we focus our attention on the half-filled case, thus the chemical potential $\mu = 0$. The coupling between a pair of localized spins at $\mathbf{R}_i$ and $\mathbf{R}_j$ is given by [28],

$$J_{ij} = -\frac{(JS)^2}{2\pi} \int_{-\infty}^{+\infty} \Im[G^{\uparrow}_{ij}(\omega) G^{\downarrow}_{ji}(\omega)] f(\omega) d\omega. \tag{2}$$

The Green's function $\widehat{G}^{\sigma}(\omega) = (\omega + i\eta - \widehat{H}^{\sigma})^{-1}$, where $\widehat{H}^{\sigma}$ is the Hamiltonian in the spin sector σ ($\sigma = \uparrow, \downarrow$). In addition, η mimics an infinitesimal inelastic scattering rate and $f(\omega) = \frac{1}{e^{\beta(\omega-\mu)}+1}$ is the Fermi-Dirac distribution. $J_{ij} \geqslant 0$ (resp. $J_{ij} \leqslant 0$) means antiferromagnetic (respectively, ferromagnetic) coupling. Notice that Eq. (2) is derived for classical spins and implies that the corresponding effective Heisenberg Hamiltonian reads $\frac{1}{2}\sum_{i\neq j} J_{ij} \mathbf{e}_i \cdot \mathbf{e}_j$.

The calculation of J_{ij} requires the knowledge of the ground-state (GS), hence that of the underlying localized spin texture. The spin configuration could be the state where spins are randomly oriented, it mimics the high temperature phase, but we would have to deal with this disordered system numerically only. Instead, we consider the GS at $T = 0\,K$ and restrict ourself to two different spin configurations: (i) the

*georges.bouzerar@neel.cnrs.fr

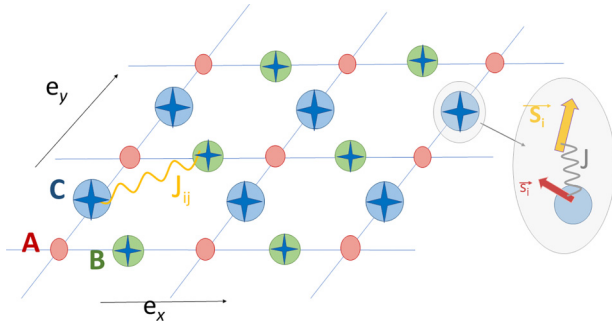

FIG. 1. Illustration of the *s-d* Lieb Model. The hoppings are restricted to nearest neighbor pairs, crosses on B (C) sites correspond to the local exchange J between the spin of the itinerant carrier ($\mathbf{s}_i$) and the localized one $\mathbf{S}_i$. J_{ij} is the magnetic couplings between pairs of localized spins.

ferromagnetic GS (F-GS) where spins on B and C sublattices are parallel and (ii) the antiferromagnetic GS (AF-GS) where spins are anti-parallel. Figure 2 shows the GS energy per unit cell E_{GS}/N (N is the number of unit cells) as a function of JS for both spin configurations. First, as expected E_{GS}/N is an even function of JS. Secondly, for $JS \neq 0$, F-GS has the lowest energy and the energy difference between these two spin configurations increases as $|JS|$ increases.

Although F-GS has the lowest energy, we discuss the nature of the couplings for F-GS and AF-GS. The data are depicted in Fig. 3. In both cases, the couplings are always ferromagnetic. Finding ferromagnetic (B, C) couplings for AF-GS contradicts an antiferromagnetic ordering at $T = 0\,K$. Thus, even if we start with the wrong GS, the calculated couplings reveal the correct magnetic order. Interestingly, the couplings are found significantly larger for AF-GS than for F-GS. More precisely, for short distances they are about 10

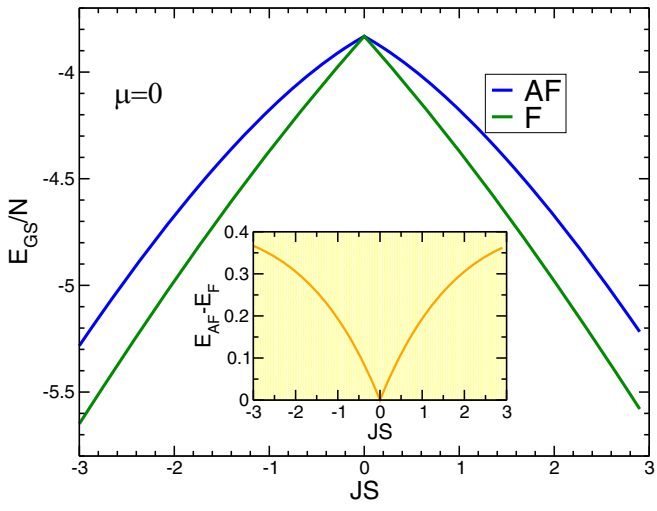

FIG. 2. Ground-state energy per unit cell E_{GS}/N as a function of JS. *AF* denotes the antiferromagnetic spin texture: $\mathbf{S}_i = +S\mathbf{e}_z$ (respectively, $\mathbf{S}_i = -S\mathbf{e}_z$) on B (resepctively, C) sublattice. *F* is the ferromagnetic spin texture, $\mathbf{S}_i = +S\mathbf{e}_z$ on both sublattices. The inset represents the energy difference between these two spin configurations.

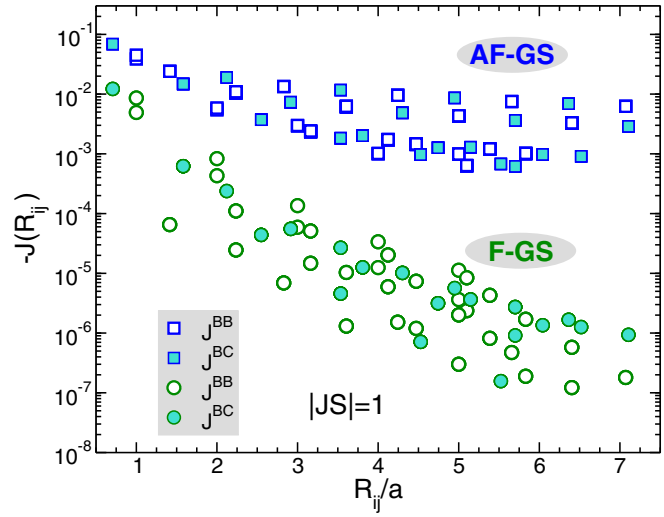

FIG. 3. Couplings (in units of t) as a function of the distance for $|JS| = t$. The circles (respetively, squares) correspond to the ferromagnetic (respectively antiferromagnetic) spin texture. The open (respectively filled) symbols correspond to (B, B) [respectively (B, C)] couplings.

times larger in the first than in the second case, it becomes 3 orders of magnitude when $R_{ij} \geqslant 4\,a$. The plotted data are obtained for $|JS| = t$ but our conclusions are general. From now on, we consider that F-GS is the GS at $T = 0\,K$. Now, we propose to discuss in details the nature of the couplings and their interband contributions. For that purpose, we first focus our attention on (B,B) pairs. For a given distance R, we write $J^{BB} = \sum_{a,b} J^{BB}_{a,b}$, where a (respectively, b) is the band index in the spin $\uparrow$-sector (respectively, $\downarrow$-sector). a and b are $-$, 0 and $+$, they correspond respectively to the lower dispersive band (DB), to the FB and to the upper DB as illustrated in Fig. 4(a). J^{BB} along the x axis and its different contributions are depicted in Fig. 4(b)–4(d) for $|JS|/t = 0.1$, 1 and 10. The five nonvanishing terms correspond to the (a,b) pairs: $(-, 0)$, $(-, +)$, $(0, 0)$, $(+, -)$ and $(0, +)$. $J^{BB}_{-,0}$ and $J^{BB}_{0,+}$ are found antiferromagnetic and for symmetry reasons, identical. In contrast, the other three terms $J^{BB}_{-,+}$, $J^{BB}_{+,-}$ and $J^{BB}_{0,0}$ are ferromagnetic. In the weak coupling regime ($|JS| = 0.1\,t$), the dominant contribution to J^{BB} is $J^{BB}_{0,0}$ which is orders of magnitude larger than the other contributions. A fit of the data plotted in Fig. 4(b), for $R/a \gg 1$, shows that $J^{BB} \propto 1/R^4$. In the intermediate regime ($|JS| = t$), the situation differs. For short distances J^{BB} reduces to $J^{BB}_{0,0}$ while for larger ones it coincides with $J^{BB}_{+,-}$ and the sum $J^{BB}_{-,0} + J^{BB}_{-,+} + J^{BB}_{0,0} + J^{BB}_{0,+}$ vanishes. Finally, for $|JS| \gg t$, these four contributions cancel out each other for any distance and $J^{BB} \approx J^{BB}_{+,-}$. A fit of the data reveals a faster decay than in the weak coupling regime, $J^{BB} \propto 1/R^6$. These features are discussed in more details in the following. Notice as well, that our findings are general and valid for other directions and pairs of atoms.

To shed light on our numerical results, we go further and analytically derive the couplings in the weak and strong coupling regime. Details can be found in the Supplemental Material (SM) [29]. Let us start with the weak coupling regime ($|JS| \ll t$) for which we only focus on

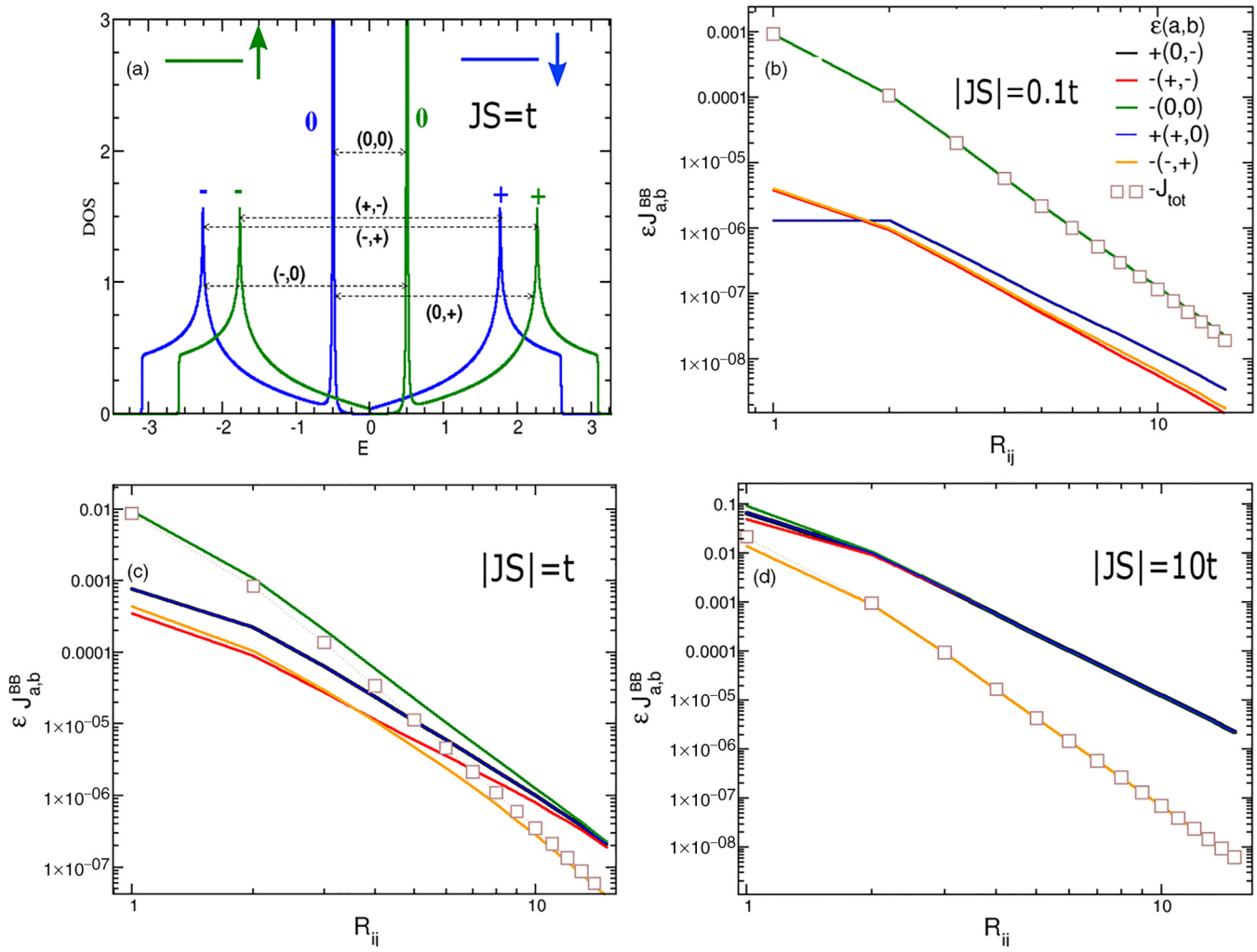

FIG. 4. (a) Density of states as a function of the energy for $JS = t$. (b)–(d) (B,B) coupling (J_{tot}) and its different contributions ($J_{a,b}$) along the x axis as a function of the distance, for three different values of $|JS|/t$ (0.1, 1 and 10). The coefficient $\epsilon = 1$ for antiferromagnetic couplings and $\epsilon = -1$ for ferromagnetic ones. a (respectively, b) is the band index in the $\uparrow$ (respectively, $\downarrow$) spin-sector and a and b can be $-$ (lower dispersive band), $+$ (upper dispersive band) and 0 (flat band).

the FB-FB contribution. The FB eigenvalues and eigenstates for both spin sectors are, $E_0^\sigma = \pm\frac{JS}{2} = \pm\Delta$ where $+$ (respectively,$-$) corresponds to $\sigma = \uparrow$ (respectively, $\sigma = \downarrow$) and $\langle\Psi_0^\sigma| = (0, \frac{f_y}{s}, -\frac{f_x}{s})$, where $f_\lambda = -2t\cos(k_\lambda a/2)$, with $\lambda = x, y$ and $s(\mathbf{k}) = \sqrt{f_x^2(\mathbf{k}) + f_y^2(\mathbf{k})}$. Starting from the definition of the couplings, we get

$$J_{0,0}^{XY}(\mathbf{R}) = -\frac{1}{2}|JS|\left|\frac{1}{N}\sum_{\mathbf{k}}\frac{f_{XY}(\mathbf{k})}{s^2(\mathbf{k})}e^{i\mathbf{k}.\mathbf{R}}\right|^2, \tag{3}$$

where $f_{XY}(\mathbf{k}) = f_y^2(\mathbf{k})$, $f_x^2(\mathbf{k})$ and $f_x(\mathbf{k}).f_y(\mathbf{k})$ for, respectively, $(X, Y) = (B, B)$, (C, C) and (B, C). Eq. (3) shows that for any pairs of atoms, $J_{0,0}^{XY}(\mathbf{R})$ is always ferromagnetic and varies linearly with $|JS|$. This is so because JS appears in the denominator of $\Im[G_{ij}^{fb\uparrow}(\omega)G_{ji}^{fb\downarrow}(\omega)]$, where $G_{ij}^{fb\sigma}$ is the FB contribution to the Green's function in the σ sector.

This contrasts with the standard weak coupling regime which leads to a $(JS)^2$ dependency of the couplings. It simply means that the perturbative calculation breaks down in the presence of FBs. Indeed, the FB-FB contribution is simply absent in the perturbative calculation since the Green's functions used are those corresponding to $JS = 0$. In a recent work, within such an approach, it has been shown that the FB-DB terms introduce strong frustration effects [30]. This is still partly correct, the FB-DB contributions are antiferromagnetic and for $|JS| \leqslant t$ they scale as $(JS)^2$. However, $J_{0,0}^{XY}(\mathbf{R})$ largely dominates and washes out completely the frustration effects. This explains why in the numerical data of Fig. 4(b), the FB-FB term is much larger that the other contributions by at least one order of magnitude. We should stress the fact that Eq. (3) is valid for any $|JS|$. It could have suggested a divergence of the couplings in the limit $|JS| \to \infty$, but as it has been shown [see Fig. 4(d)] the other contributions cancel out the divergence. The complete analytical calculations as detailed in Ref. [29] lead to

$$J_{0,0}^{XY}(\mathbf{R}) = -|JS|\frac{a^4}{8\pi^2 R^4}g_{XY}(\theta), \tag{4}$$

where $g_{XY}(\theta) = \cos^2(2\theta)$ for (X,Y) = (B,B) or (C,C), and $g_{XY}(\theta) = \sin^2(2\theta)$ for (X,Y)=(B,C). θ is the angle between $\mathbf{R}$ and the x axis. Eq. (4) clearly explains the $1/R^4$ decay of the couplings found in the numerical calculations. Let us define the dimensionless quantity $C^0 = \frac{J^{BB}_{0,0}}{|JS|} \cdot [\frac{R}{a}]^4$. A fit of the numerical data plotted in Fig. 4(b) gives $C^0 = -0.0123$ which agrees very well with the analytical result $C^0 = -0.0126$.

We switch to the strong coupling regime ($|JS| \gg t$) for which the couplings reduce to $J^{XY}_{-,+}$. The energy of the DBs in each spin sector are $E^{\uparrow}_{\pm} = -g_{\mp}$ and $E^{\downarrow}_{\pm} = g_{\pm}$ where $g_{\pm} = \frac{1}{2}[-\Delta \pm \sqrt{\Delta^2 + 4s^2}]$. The corresponding eigenvectors are, respectively, $\langle\Psi^{\uparrow}_{\pm}| = \frac{1}{D_{\pm}}(g_{\pm}, f_x, f_y)$ and $\langle\Psi^{\downarrow}_{\pm}| = \frac{1}{D_{\mp}}(-g_{\mp}, f_x, f_y)$, where $D_{\pm} = \sqrt{s^2 + g^2_{\pm}}$. Because, the full calculation of $J^{XY}_{-,+}$ is lengthy, the details can be found in the the SM [29]. For $|JS| \gg t$, we find

$$J^{BB}_{-,+}(\mathbf{R}) = -\frac{1}{\pi^2}(4\cos^2(\theta) - 1)^2 \frac{a^6}{R^6}\frac{t^2}{|JS|}, \tag{5}$$

$$J^{BC}_{-,+}(\mathbf{R}) = -\frac{3}{\pi^2}\sin^2(2\theta)\frac{a^6}{R^6}\frac{t^2}{|JS|}. \tag{6}$$

Notice that $J^{CC}_{-,+}(\mathbf{R})$ is straightforwardly obtained by replacing in $J^{BB}_{-,+}$ θ by $\frac{\pi}{2} + \theta$. These expressions clearly explain the $1/R^6$ decay of the (B,B) couplings observed in the numerical calculations. As before, we define the dimensionless variable $C^{\infty} = J^{BB}_{-,+} \cdot [\frac{R}{a}]^6 \cdot \frac{|JS|}{t^2}$. From a fit of the numerical data plotted in Fig. 4(c) we obtain $C^{\infty} = -0.71$, while Eq. (5) gives for $\theta = 0$, $C^{\infty} = -0.91$. The agreement between analytical and numerical calculations is not as good as that found for $|JS| \ll t$. However, for other directions, the agreement is much better. For $\theta = \frac{\pi}{2}$, Eq. (5) gives $C^{\infty} = -0.101$ and from the numerical data one gets $C^{\infty} = -0.102$. On the other hand, for $J^{BC}_{-,+}$ an excellent agreement is found for any values of θ. More details are available in the SM [29].

In order to derive the crossover temperature $T^{\star}_C$, we now turn to the calculation of the magnetic excitation spectrum. It is important to point out that, because the couplings decay sufficiently rapidly, in other words $\sum_{\mathbf{R}} J^{XY}(\mathbf{R})R^2$ is finite for any (X, Y) pair, the Mermin-Wagner theorem [23] implies that in the thermodynamic limit (system size $\to \infty$) the Curie temperature (T_C) vanishes. A finite T_C in 2DM is possible only in the presence of anisotropy, which opens a gap in the Goldstone mode. However, even in absence of anisotropy, for a finite system one can define a size dependent crossover temperature $T^{\star}_C$. A relevant question is, what is the order of magnitude of $T^{\star}_C$ for a micrometer-sized sample which is typically that of samples realized in laboratories. An appropriate tool to estimate $T^{\star}_C$ is the random phase approximation (RPA) [31,32]. In diluted magnetic semiconductors, the comparison with Monte Carlo simulation has revealed that RPA is reliable and accurate [33]. It should be pointed out that it has been demonstrated by a direct comparison between the full Monte Carlo study (itinerant carriers coupled to classical spins) of a similar Hamiltonian to that given in Eq. (1) that the two-step approach is reliable and accurate. We emphasize that it is the case even in the presence of disorder [34].

To proceed with the RPA approach, the Heisenberg Hamiltonian is written

$$H^H = \frac{1}{2}\sum_{i\neq j} \mathcal{J}_{ij}\mathbf{S}_i \cdot \mathbf{S}_j, \tag{7}$$

where the couplings $\mathcal{J}_{ij} = J_{ij}/S^2$. Notice that, the RPA involves the presence of commutators between the localized spins and the Heisenberg Hamiltonian, thus $\mathbf{S}_i$ is treated as quantum operator. It should be emphasized that in the case of ferromagnetism the nature (quantum or classical) of the localized spin has only a minor impact. Indeed, let us recall the results concerning the nearest-neighbor Heisenberg Hamiltonian on the simple cubic lattice. We first define the ratio $K_c = T_C/(JS(S+1))$ where T_C is the Curie temperature. First, from classical Monte Carlo simulations (CMC) which means $S = \infty$ and JS^2 is constant, it has been found that $K_c = 1.44$ [35]. On the other hand, from quantum Monte Carlo calculations (QMC) it has been shown that $K_c = 1.15$ for $S = 1/2$ [36]. These results should be compared to high temperature expansion calculations for which one finds $K_c = 1.15$ for $S = 1/2$ [37], $K_c = 1.3$ for $S = 1$ [38] and $K_c = 1.4$ for $S = \infty$ [38]. Finally, the RPA leads to $K_c = 1.33$ for any value of S [31,32]. To summarize, from QMC, CMC, HTE, and RPA one clearly concludes that the nature of the spin has a negligible impact since $K_c = 1.35 \pm 0.05$ for $S \geqslant 1$.

To calculate the magnetic properties, we use the equation of motion method applied to the retarded spin Green's function, $G^S_{ij,XY}(\omega) = \int_{-\infty}^{+\infty} G^S_{ij,XY}(t)e^{i\omega t}dt$ where $G^S_{ij,XY}(t) = -i\theta(t)\langle[S^+_{X,i}, S^-_{Y,j}]\rangle$ and, $\langle ...\rangle$ denotes the thermal average. We only present the main results, the full procedure is detailed in Ref. [29]. As expected, we find two magnon branches, $\omega^{\pm}_{\mathbf{q}} = \langle S^z\rangle E^{\pm}_{\mathbf{q}}$, where $-$' is the acoustic mode and $'+'$ is the optical one, and

$$E^{\pm}_{\mathbf{q}} = f^{\mathbf{q}}_{+} \pm \sqrt{(f^{\mathbf{q}}_{-})^2 + \left(f^{\mathbf{q}}_{BC}\right)^2}, \tag{8}$$

where $f^{\mathbf{q}}_{+} = \frac{1}{2}(f^{\mathbf{q}}_{BB} + f^{\mathbf{q}}_{CC})$ and $f^{\mathbf{q}}_{-} = \frac{1}{2}(f^{\mathbf{q}}_{BB} - f^{\mathbf{q}}_{CC})$ with $f^{\mathbf{q}}_{XX} = -\sum_Y \bar{\mathcal{J}}^{XY}(\mathbf{0}) + \bar{\mathcal{J}}^{XX}(\mathbf{q})$ $(X = B, C)$, we have defined as well $\bar{\mathcal{J}}^{XY}(\mathbf{q}) = \sum_{\mathbf{R}} e^{i\mathbf{q}.\mathbf{R}}\mathcal{J}^{XY}(\mathbf{R})$ and $f^{\mathbf{q}}_{BC} = \bar{\mathcal{J}}^{BC}(\mathbf{q})$. As it is shown in Ref. [29], the crossover temperature is given by

$$k_B T^{\star}_C = \frac{1}{3}\left(1 + \frac{1}{S}\right)\left[\frac{1}{N}\sum_{\mathbf{q}\neq\mathbf{0},\lambda=\pm}\frac{A^{\lambda}_{\mathbf{q}}}{S^2 E^{\lambda}_{\mathbf{q}}}\right]^{-1}. \tag{9}$$

$A^{\pm}_{\mathbf{q}}$ is the spectral weight on each magnon branch. Equation (9) can be written $T^{\star}_C = (1 + \frac{1}{S})T^{\star,cl}_C$, where $T^{\star,cl}_C$ is the crossover temperature for classical spins ($S \to \infty$). Let us discuss the size dependence of $T^{\star,cl}_C$. We consider square shaped flakes of size $La \times La$. For small $|\mathbf{q}|$ we have, $A^{\pm}_{\mathbf{q}} \approx 1/2$, $E^{+}_{\mathbf{q}} \approx E^{+}_{\mathbf{0}}$ and $E^{-}_{\mathbf{q}} \approx Dq^2$, where D is the spin stiffness of the acoustic mode, leading to $\frac{1}{N}\sum_{\mathbf{q}\neq\mathbf{0},\lambda=\pm}\frac{A^{\lambda}_{\mathbf{q}}}{S^2E^{\lambda}_{\mathbf{q}}} \approx \frac{1}{2S^2}[\frac{1}{E^{+}_{\mathbf{0}}} + \frac{a^2}{2\pi D}\ln(\frac{Q_C}{q_{\min}})]$, where Q_C is a cutoff, and $Q_{\min} = \frac{2\pi}{La}$ being the smallest non zero momentum. Then, Eq. (9) becomes

$$k_B T^{\star,cl}_C = \frac{2S^2}{A + B\ln\left(\frac{L}{2\pi}\right)}. \tag{10}$$

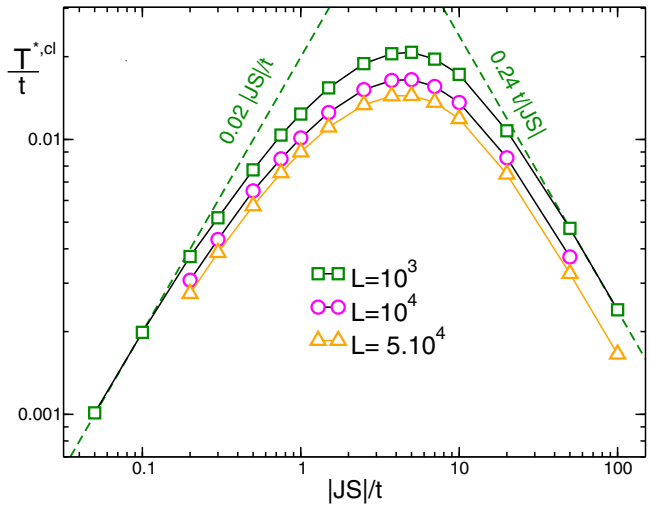

FIG. 5. Crossover temperature $T_C^{\star,cl}$ as a function of $|JS|$ for three different sizes $L = 10^3$, 10^4 and $5.\,10^4$. The green dashed lines are fits for the weak and strong coupling regimes for the data obtained for $L = 10^3\,a$.

$A = \frac{1}{E_0^+} + \frac{a^2}{2\pi D}\ln(a.Q_C)$ and $B = \frac{a^2}{2\pi D}$. As expected, $T_C^{\star,cl}$ decays slowly as $1/\ln(L)$, and in accordance with the MW theorem, it vanishes in the limit $L \to \infty$. In the presence of a small anisotropy leading to a gap (Δ) opening, $\ln(\frac{L}{2\pi})$ is replaced by $\frac{1}{2}\ln(\frac{D}{\Delta a^2})$ and $T_C^{\star,cl}$ becomes the true Curie temperature. To show the accuracy of RPA, we compare our $T_C^{*,cl}$ for the nearest neighbor Heisenberg Hamiltonian on the square lattice with that obtained from Monte Carlo simulations (MC) [22]. The system considered is a $1\mu m \times 1\mu m$ flake with a lattice spacing $a = 4\mathring{A}$. Using Eq. (10), we get $T_C^{\star,RPA} \approx 0.58\,\mathrm{J}$ while it has been found $T_C^{\star,MC} \approx 0.535\,\mathrm{J}$, where J denotes the nearest neighbor coupling between the classical spins. We observe that the agreement between RPA and MC is surprisingly good. We confidently return to our system. In Fig. 5, $T_C^{\star,cl}$, calculated numerically is plotted as a function of $|JS|$ for three different sizes, the biggest system contains 12.5 billions of atoms. As can be seen, an increase of L as a small impact on $T_C^{\star,cl}$. This is consistent with the $\ln(L)$ dependency in Eq. (10). We now estimate the crossover temperature in mesoscopic samples. We assume a lattice spacing a of about 3 $\mathring{A}$ and choose for t a typical value of 1 eV, we recall that in graphene $t \approx 2.7$ eV. From Fig. 5 the maximum of the crossover temperature $T^{\star}_{\max}$ in a $3\,\mu m \times 3\,\mu m$ sample is 410, and 342 K for, respectively $S = 1/2$, $S = 1$ and $S = 3/2$. These temperatures are beyond room temperature and one order of magnitude higher than those reported in various 2DMs such as $Cr_2Ge_2Te_6$ [15] and Fe_3GeTe_2 [17].

In conclusion, FB states could pave the way to ambient ferromagnetism in 2D materials. It is revealed, in the weak and intermediate coupling regime, that the magnetic exchanges between localized spins are largely dominated by the ferromagnetic FB-FB contribution which scales linearly with the local coupling, contrasting with the standard quadratic dependence of the other contributions. Using reasonable physical parameters, we find that crossover temperatures well beyond 300 K could be reached in micrometer-sized systems opening interesting avenues towards technological applications.

[1] D. Leykam, A. Andreanov, and S. Flach, Adv. Phys. X **3**, 1473052 (2018).
[2] L. Balents, C. R. Dean, D. K. Efetov, and A. F. Young, Nat. Phys. **16**, 725 (2020).
[3] E. Tang, J.-W. Mei, and X.-G. Wen, Phys. Rev. Lett. **106**, 236802 (2011).
[4] T. Neupert, L. Santos, C. Chamon, and C. Mudry, Phys. Rev. Lett. **106**, 236804 (2011).
[5] S. Miyahara, S. Kusuta, and N. Furukawa, Physica C **460-462**, 1145 (2007).
[6] Y. Cao *et al.*, Nature (London) **556**, 43 (2018).
[7] M. Yankowitz *et al.*, Science **363**, 1059 (2019).
[8] Z. Lin, J.H. Choi, Q. Zhang, W. Qin, S. Yi, P. Wang, L. Li, Y. Wang, H. Zhang, Z. Sun *et al.* Phys. Rev. Lett. **121**, 096401 (2018).
[9] J.-X. Yin, Nat. Phys. **15**, 443 (2019).
[10] H. Tasaki, Prog. Theor. Phys. **99**, 489 (1998).
[11] G. Bouzerar and D. Mayou, Phys. Rev. Res. **2**, 033063 (2020); Phys. Rev. B **103**, 075415 (2021).
[12] A. Ferreira and E. R. Mucciolo, Phys. Rev. Lett. **115**, 106601 (2015).
[13] M. Vigh, L. Oroszlany, S. Vajna, P. San-Jose, G. David, J. Cserti, and B. Dora, Phys. Rev. B **88**, 161413(R) (2013).
[14] G. Bouzerar, Phys. Rev. B **106**, 125125 (2022).
[15] C. Gong, L. Li, Z. Li *et al.*, Nature (London) **546**, 265 (2017).
[16] B. Huang, G. Clark, E. Navarro-Moratalla *et al.*, Nature (London) **546**, 270 (2017).
[17] Y. Deng, Y. Yu, Y. Song *et al.*, Nature (London) **563**, 94 (2018).
[18] Q. H. Wang *et al.*, ACS Nano **16**, 6960 (2022).
[19] Y. Ma, J. Yu, and H. Thomas, 2D Mater. **4**, 025111 (2017).
[20] J. L. Miller, Phys. Today **70**, 7 (2017).
[21] M. Gibertini, M. Koperski, A. F. Morpurgo, and K. S. Novoselov, Nat. Nanotechnol. **14**, 408 (2019).
[22] S. Jenkins, L. Rózsa, U. Atxitia *et al.*, Nat. Commun. **13**, 6917 (2022).
[23] N. D. Mermin and H. Wagner, Phys. Rev. Lett. **17**, 1133 (1966).
[24] H. E. Stanley and T. A. Kaplan, Phys. Rev. Lett. **17**, 913 (1966).
[25] S. H. Shenker and J. Tobochnik, Phys. Rev. B **22**, 4462 (1980).
[26] H. W. J. Blöte, W. Guo, and H. J. Hilhorst, Phys. Rev. Lett. **88**, 047203 (2002).
[27] W. Jiang, H. Huang, and F. Liu, Nat. Commun. **10**, 2207 (2019).
[28] A. I. Lichtenstein, M. I. Katsnelson, V. A. Gubanov, J. Phys. F. **14**, L125 (1984); M. I. Katsnelson and A. I. Lichtenstein, Phys. Rev. B **61**, 8906 (2000).
[29] See Supplemental Material at http://link.aps.org/supplemental/10.1103/PhysRevB.107.184441, which contains the calculation of the magnetic couplings in the weak and strong coupling regime, and that of the crossover temperature.
[30] G. Bouzerar, Phys. Rev. B **104**, 155151 (2021).

[31] S. V. Tyablicov, *Methods in Quantum Theory of Magnetism* (Plenum, New York, 1967).
[32] H. B. Callen, Phys. Rev. **130**, 890 (1963).
[33] R. Bouzerar, D. May, U. Low, D. Machon, P. Melinon, S. Zhou, and G. Bouzerar, Phys. Rev. B **94**, 094437 (2016).
[34] G. Bouzerar and O. Cépas, Phys. Rev. B **76**, 020401(R) (2007).
[35] P. Peczak, A. M. Ferrenberg, and D. P. Landau, Phys. Rev. B **43**, 6087 (1991).
[36] A. J. F. de Souza, U. M. S. Costa, and M. L. Lyra, Phys. Rev. B **62**, 8909 (2000).
[37] J. Oitmaa and E. Bornilla, Phys. Rev. B **53**, 14228 (1996).
[38] A. Lohmann, H.-J. Schmidt, and J. Richter, Phys. Rev. B **89**, 014415 (2014).